Tidal dissipation in rotating low-mass stars and implications for the orbital evolution of close-in planets. I. From the PMS to the RGB at solar metallicity

F. Gallet, E. Bolmont, S. Mathis, C. Charbonnel, L. Amard

▶ To cite this version:

Astronomy & Astrophysics

Tidal dissipation in rotating low-mass stars and implications for the orbital evolution of close-in planets

I. From the PMS to the RGB at solar metallicity

F. Gallet[1], E. Bolmont[2,3], S. Mathis[2], C. Charbonnel[1,4], and L. Amard[1,5]

[1] Department of Astronomy, University of Geneva, Chemin des Maillettes 51, 1290 Versoix, Switzerland
e-mail: florian.gallet@unige.ch
[2] Laboratoire AIM Paris-Saclay, CEA/DRF – CNRS – Univ. Paris Diderot – IRFU/SAp, Centre de Saclay, 91191 Gif-sur-Yvette Cedex, France
[3] NaXys, Department of Mathematics, University of Namur, 8 Rempart de la Vierge, 5000 Namur, Belgium
[4] IRAP, UMR 5277, CNRS and Université de Toulouse, 14 av. E. Belin, 31400 Toulouse, France
[5] LUPM UMR 5299 CNRS/UM, Université de Montpellier, CC 72, 34095 Montpellier Cedex 05, France

ABSTRACT

Context. Star-planet interactions must be taken into account in stellar models to understand the dynamical evolution of close-in planets. The dependence of the tidal interactions on the structural and rotational evolution of the star is of particular importance and should be correctly treated.
Aims. We quantify how tidal dissipation in the convective envelope of rotating low-mass stars evolves from the pre-main sequence up to the red-giant branch depending on the initial stellar mass. We investigate the consequences of this evolution on planetary orbital evolution.
Methods. We couple the tidal dissipation formalism previously described to the stellar evolution code STAREVOL and apply this coupling to rotating stars with masses between 0.3 and 1.4 $M_\odot$. As a first step, this formalism assumes a simplified bi-layer stellar structure with corresponding averaged densities for the radiative core and the convective envelope. We use a frequency-averaged treatment of the dissipation of tidal inertial waves in the convection zone (but neglect the dissipation of tidal gravity waves in the radiation zone). In addition, we generalize a recent work by following the orbital evolution of close-in planets using the new tidal dissipation predictions for advanced phases of stellar evolution.
Results. On the pre-main sequence the evolution of tidal dissipation is controlled by the evolution of the internal structure of the contracting star. On the main sequence it is strongly driven by the variation of surface rotation that is impacted by magnetized stellar winds braking. The main effect of taking into account the rotational evolution of the stars is to lower the tidal dissipation strength by about four orders of magnitude on the main sequence, compared to a normalized dissipation rate that only takes into account structural changes.
Conclusions. The evolution of the dissipation strongly depends on the evolution of the internal structure and rotation of the star. From the pre-main sequence up to the tip of the red-giant branch, it varies by several orders of magnitude, with strong consequences for the orbital evolution of close-in massive planets. These effects are the strongest during the pre-main sequence, implying that the planets are mainly sensitive to the star's early history.

Key words. hydrodynamics – waves – planet-star interactions – stars: evolution – stars: rotation

1. Introduction

Thanks to space observatories and to the increase in the precision of modern techniques (e.g. radial velocity and transit methods), we now have access to a huge number of exoplanets that belong to a wide variety of star–planet system configurations where the host stars range from M red dwarf to intermediate-mass A-type stars (Fabrycky et al. 2014). Among these discovered exoplanets, a fairly large number of them are found close to their host stars, as is the case for the well-known hot-Jupiter class exoplanets (Mayor & Queloz 1995; Charbonneau et al. 2000).

The presence of planets is usually not taken into account in the numerical codes dealing with the evolution of stellar rotation, such as angular momentum evolution codes (e.g. Reiners & Mohanty 2012; Gallet & Bouvier 2013, 2015; Johnstone et al. 2015; Lanzafame & Spada 2015) or stellar evolution codes including angular momentum transport (e.g. Endal & Sofia 1976, 1981; Pinsonneault et al. 1990; Brott et al. 2011; Amard et al. 2016; Choi et al. 2016). The

increasing number of detected and confirmed exoplanets, especially because most of them are found close to their host star, means that star-planet interactions should not be neglected (as shown by the studies of Strugarek et al. 2014; Strugarek 2016, for the magnetic interactions; and of Bolmont & Mathis 2016, for tidal interactions). Indeed, in these close-in configurations, the dissipation of tidal waves inside the turbulent convective envelope of low-mass stars is thought to strongly affect the orbit of the surrounding planet (Jackson et al. 2008; Husnoo et al. 2012; Lai 2012; Guillot et al. 2014), the spin-orbit inclination (Barker & Ogilvie 2009; Winn et al. 2010; Albrecht et al. 2012), and – in the case of a massive planet – the rotational evolution of the star (Ogilvie & Lin 2007; Bolmont et al. 2011, 2012; Albrecht et al. 2012; Ogilvie 2014; Auclair-Desrotour et al. 2014; Mathis 2015; Bolmont & Mathis 2016) and possibly its internal structure (de Boer & Seggewiss 2008).

In stars, there are two components to describe the tidal interaction, equilibrium tides and dynamical tides. Equilibrium tides

correspond to a large-scale hydrostatic adjustment of a body and the resulting flow due to the gravitational field of a given companion (Zahn 1966; Remus et al. 2012). It is usually employed in the framework of the constant time lag model (see Mignard 1979; Hut 1981; Eggleton et al. 1998; Bolmont et al. 2011, 2012), which allows a fast computation of the orbital evolution of the planet and works for all eccentricities (Hut 1981; Leconte et al. 2010). In this model, the dissipation of the kinetic energy of the equilibrium tide inside the star is often taken to be constant throughout the system evolution and calibrated on observations (Hansen 2010, 2012). While considering such a constant equilibrium tide dissipation is a sensible assumption, several studies have shown that this quantity might vary during the different phases of stellar evolution. For example, Zahn & Bouchet (1989) showed that the dissipation of the equilibrium tide by the turbulent friction in the convective envelope of late-type stars is strongest during their PMS. Using this theoretical framework, Villaver & Livio (2009, see also Verbunt & Phinney 1995) recalled that the variation of the semi-major axis of a planet induced by such friction can be expressed as a function of the ratio of the mass of the convective envelope to the total mass of the star, the ratio between the radius of the star and the orbital semi-major axis (to the power 8), and finally of a power of the ratio between the tidal period and the convective turnover timescale. This allows the loss of efficiency of tidal friction to be modelled for rapid tides (e.g. Zahn 1966; Goldreich & Keeley 1977). Because of the variations of these quantities during post-MS phases (e.g. Charbonnel et al. 2017), this could lead to a more efficient dissipation than during the MS. Finally, Mathis et al. (2016) demonstrated that the action of rotation on convection deeply modifies the turbulent friction it applies on the equilibrium tide. In the regime of fast rotation, which corresponds to the end of PMS and early MS phase, the friction is several orders of magnitude lower than in a model ignoring rotation. This may lead to a loss of efficiency of the dissipation of the equilibrium tide. This shows that care should be taken when assuming a calibrated constant dissipation of the equilibrium tide during the evolution of stars.

On the other hand, dynamical tides correspond to the excitation of tidal waves inside the star (Zahn 1975; Ogilvie & Lin 2007). In the dynamical tide formalism, the tidal dissipation in the convective envelope of low-mass stars is due to the action of the convective turbulent friction applied on tidal inertial waves (mechanical waves that are generated inside rotating fluid bodies) driven by the Coriolis acceleration (Ogilvie & Lin 2007; Mathis et al. 2016). In the radiative layers, the dissipation is due to thermal diffusion and breaking mechanisms acting on gravito-inertial waves (e.g. Zahn 1975; Terquem et al. 1998; Barker & Ogilvie 2010).

The properties of a star, its internal structure (relative masses and radii of the radiative core and convective envelope), and its rotation rate actively evolve throughout the stellar life. The temporal evolution of the radius and mass of the radiative core and of the surface rotation rate has strong consequences on the evolution of the amplitude of the tidal dissipation in stars during their evolution (Zahn 1966, 1975, 1977; Ogilvie & Lin 2007; Siess et al. 2013; Mathis 2015; Mathis et al. 2016). This could explain observations of star–planet and binary-star systems that show a range of tidal dissipation varying over several orders of magnitude, as reported by Ogilvie (2014). Moreover, the tidal dissipation strongly impacts the dynamical evolution of planetary systems along the evolution of their host stars (e.g. Bolmont et al. 2012; Bolmont & Mathis 2016). We thus need to

take into account its potential variations as a function of stellar age using the best available ab initio modelling.

The work of Mathis (2015) constituted the first step towards a complete description of tidal dissipation along stellar evolution. Using a simplified two-layer model, as in Ogilvie (2013), Mathis (2015) followed the dissipation of the dynamical tide inside the convective envelope along the standard stellar evolution tracks of Siess et al. (2000). Bolmont & Mathis (2016) then included in their orbital evolution code (Bolmont et al. 2011, 2012) the prescription for the dynamical tide of Mathis (2015) coupled to a simplified description of the evolution of the stellar surface rotation rate. This work led to the complete re-evaluation of the effects of star–planet tidal interactions on the orbital evolution of massive close-in planets. In particular, Bolmont & Mathis (2016) reported outward and inward migrations of close-in hot Jupiters orbiting solar-type stars while little or no evolution was initially found when including only the equilibrium tide component. While these pioneer developments represent an important step forward in understanding the complexity of the tidal interactions between stars and planets, we now need to properly account for the evolution of the rotation of the star and its interconnection with secular structure variations. This is particularly important for characterizing the orbital evolution of short-period systems. Actually, by using a constant (in time) quality factor (Goldreich & Soter 1966) or time lag formalism, it is not possible to explain the hot-Jupiter desert that we observe around rapidly rotating stars (Lanza & Shkolnik 2014; Teitler & Königl 2014; McQuillan et al. 2013; Mazeh et al. 2016). Providing a simplified but realistic evolution of the tidal dissipation is crucial to predicting the position at which planets are at any time and to rapidly exploring the effects of initial conditions on their orbital evolution and on possible planet engulfment that is expected to strongly affect the surface rotation of hot stars (Siess & Livio 1999; Privitera et al. 2016a,b). Such tools will be essential for the preparation and the exploitation of future observations with CHEOPS (Broeg et al. 2015), TESS (Ricker et al. 2015), and SPIRou (Moutou et al. 2015).

In this context, the originality of the present work is that we introduce for the first time in a stellar evolution code (STAREVOL) the prescription of Mathis (2015) for the dissipation of the dynamical tide inside stellar convective envelopes. This allows us to follow this quantity self-consistently together with the secular and rotational history of stars, from the pre-main sequence (PMS) up to the red-giant branch (RGB). We also take into account the equilibrium tide using the constant time lag model. This paper is organized as follows. In Sect. 2 we recall the formalism and the assumptions used to analytically express the frequency-averaged tidal dissipation (see Ogilvie 2013) and the microphysics and assumptions used in STAREVOL. In Sect. 3 we describe the evolution of the dissipation as a function of mass, evolutionary phase, and rotation for stars ranging between 0.3 and 1.4 $M_\odot$. In Sect. 4 we show the influence of the evolving structure and tidal dissipation on the orbital evolution of close-in planets around 1 $M_\odot$ and 1.2 $M_\odot$ stars. We conclude and discuss the perspectives of this work in Sect. 5.

2. Model description

2.1. Tidal dissipation formalism

In this section we describe the method we use to couple, for the first time, the structural and rotational evolution of low-mass stars to tidal dissipation in their convective envelope.

2.1.1. Generalities

Let us consider two bodies: a deformable star and a point-mass planet. The planet exerts a differential force on the star that causes its deformation and leads to the generation of tidal flows. These tidal flows are submitted to friction in its interior (as is the case for the synchronization of massive binaries by the damping of gravity waves near the stellar surface; Goldreich & Nicholson 1989b). Part of the kinetic energy associated with the flows is converted and lost in the thermal energy inside the star, and part of it is transferred to the planet's orbit via angular momentum exchanges. These processes are governed by the tidal dissipation which depends on the dissipative processes and the stellar internal structure. The complex tidal interactions between star and planets is decomposed into the equilibrium tide and the dynamical tide (e.g. Zahn 1966, 1975, 1977; Mathis & Remus 2013; Ogilvie 2014), which are both considered in the present study.

The equilibrium non-wave-like tide corresponds to the internal large-scale flows produced by the hydrostatic adjustment of the stellar structure due to the presence of a companion (Zahn 1966; Remus et al. 2012; Ogilvie 2013). This tide is efficiently dissipated in the convective envelope of rotating low-mass stars by turbulent friction due to convection motion (Zahn 1966, 1989; Ogilvie & Lesur 2012; Mathis et al. 2016). In most of the studies of the tidal evolution of planetary systems, only the equilibrium tide is taken into account (e.g. Mignard 1979; Hut 1981; Leconte et al. 2010; Bolmont et al. 2011). In this work we model this component using the framework of the constant time lag model (see Mignard 1979; Hut 1981; Eggleton et al. 1998; Bolmont et al. 2011, 2012).

On the other hand, the dynamical tide comes from inertial waves propagating through the convective envelope that are driven by the Coriolis acceleration and excited when the tidal excitation frequency $|\omega|$ is smaller than $2\Omega_\star$, where $\Omega_\star$ is the stellar spin. The tidal frequency is defined in Ogilvie (2014) as the linear combination of the orbital and spin frequencies with small integer coefficients. If the star-planet system is coplanar and the planet is on a circular orbit, the tidal frequency can be expressed as $\omega \equiv 2(n - \Omega_\star)$, where n is the orbital frequency (Ogilvie & Lin 2004). For tidal frequencies $|\omega| > 2\Omega_\star$ the tidal dissipation is almost independent of $\Omega_\star$ at any given tidal frequency because in that regime the effect of the Coriolis force is weak (Ogilvie & Lin 2007). In the radiative core the dynamical tide is driven by internal gravity waves (see Zahn 1975, 1977; Goldreich & Nicholson 1989a,b; Terquem et al. 1998) which can be affected by the Coriolis acceleration (Ogilvie & Lin 2007).

Both the equilibrium and the dynamical tidal effects must in principle be accounted for to properly model tidal evolution (Bolmont & Mathis 2016). However, while the equilibrium tide weakly depends on the excitation frequency variation (Remus et al. 2012), the dynamical tide strongly depends on it, and also on the evolutionary stage, mass, and rotation rate of the star (see the discussion in Ogilvie & Lin 2004, 2007; Barker & Ogilvie 2010; Auclair-Desrotour et al. 2014; Witte & Savonije 2002).

The formalism associated with the dynamical tide (see Ogilvie 2013, 2014; Mathis 2015) is currently too complex to be implemented in secular orbital evolution codes (see Bolmont & Mathis 2016) and to perform wide explorations of the parameter space (planet and stellar masses, initial rotation, and orbital configurations along the whole stellar evolution). Indeed, the dynamical tide dissipation spectrum harbours complex behaviours; it evolves as a function of the stellar properties and

age, which are computationally expensive. A first step to make significant progress is to follow the evolution of the tidal dissipation using rotating stellar models, considering first the dissipation inside the convective envelope of the stars.

2.1.2. Frequency-averaged tidal dissipation

In the formalism of Ogilvie (2013) and Mathis (2015), the stellar convective envelope is assumed to be in solid-body rotation with angular velocity $\Omega_\star$. Moderate rotation is assumed, i.e. the squared ratio of $\Omega_\star$ to the critical angular velocity Ω_c is such that $(\Omega_\star/\Omega_c)^2 = \left(\Omega_\star/\sqrt{\mathcal{G}M_\star/R_\star^3}\right)^2 \equiv \epsilon^2 \ll 1$ (so as to neglect the centrifugal effect), where $\mathcal{G}$ is the gravitational constant, and $M_\star$ and $R_\star$ are the stellar mass and equatorial radius, respectively. In this article we use the two-layer model introduced in Ogilvie (2013) and Mathis (2015) to evaluate the frequency-averaged tidal dissipation in the stellar convective envelope, and we focus on solar metallicity stars with initial masses between 0.3 and 1.4 $M_\odot$. In this mass range, the convective envelope surrounds the radiative core of radius R_c and mass M_c. Both core and envelope are assumed to be homogeneous with respective average densities ρ_c and ρ_e. This constitutes a necessary first step that allows us to derive an analytical expression for the frequency-averaged dissipation and to explore a broad range of parameters. In the near future, we shall evaluate the impact of the radial variations of the density, which varies in stellar convection zones over several orders of magnitude during the evolution of stars. This may lead to weaker dissipation rates.

In the case of a coplanar star–planet system in which the orbit of the planet is circular, the frequency-averaged tidal dissipation (Ogilvie 2013; Mathis 2015) is given by

$$\langle \mathcal{D} \rangle_\omega = \int_{-\infty}^{+\infty} \mathrm{Im}\left[\mathrm{k}_2^2(\omega)\right] \frac{\mathrm{d}\omega}{\omega} = \frac{100\pi}{63}\epsilon^2 \left(\frac{\alpha^5}{1-\alpha^5}\right)(1-\gamma)^2 \quad (1)$$

$$\times (1-\alpha)^4 \left(1 + 2\alpha + 3\alpha^3 + \frac{3}{2}\alpha^3\right)^2 \left[1 + \left(\frac{1-\gamma}{\gamma}\right)\alpha^3\right]$$

$$\times \left[1 + \frac{3}{2}\gamma + \frac{5}{2\gamma}\left(1 + \frac{1}{2}\gamma - \frac{3}{2}\gamma^2\right)\alpha^3 - \frac{9}{4}(1-\gamma)\alpha^5\right]^{-2},$$

with

$$\alpha = \frac{R_c}{R_\star}, \ \beta = \frac{M_c}{M_\star}, \ \gamma = \frac{\rho_e}{\rho_c} = \frac{\alpha^3(1-\beta)}{\beta(1-\alpha^3)} < 1. \quad (2)$$

Here k_2^2 is the second-order Love number corresponding to the quadrupolar mode (k_l^m, with $l = 2$ and $m = 2$ the components of the time-dependent tidal potential proportional to the spherical harmonic Y_l^m) that gives the ratio between the perturbation of the gravitational potential induced by the presence of the planetary companion and the tidal potential evaluated at the stellar surface. Its imaginary component $\mathrm{Im}\left[k_2^2(\omega)\right]$ is a direct estimation of the tidal dissipation. The interest of this formalism is that it is possible to decompose Eq. (1) into two parts: the factor ϵ^2 on the one hand, and the part of Eq. (1) that is a unique function of α and β on the other hand. The first part takes into account the rotation rate of the star (via ϵ), and the second part only takes into account the dependence on the internal stellar structure (via the structural parameters α and β). As in Mathis (2015), we can therefore express the frequency-averaged dissipation at a fixed rotation,

$$\langle \mathcal{D} \rangle_\omega^\Omega = \epsilon^{-2}\langle \mathcal{D} \rangle_\omega = \epsilon^{-2}\left\langle \mathrm{Im}\left[k_2^2(\omega)\right]\right\rangle_\omega, \quad (3)$$

which only depends on α and β. We can also define a second frequency-averaged dissipation using the critical angular velocity of the Sun $\Omega_c^\odot$ instead of that of the star,

$$\langle \hat{\mathcal{D}} \rangle_\omega^\Omega = \hat{\epsilon}^{-2} \langle \mathcal{D} \rangle_\omega = \left(\frac{M_\star}{M_\odot} \right)^{-1} \left(\frac{R_\star}{R_\odot} \right)^3 \langle \mathcal{D} \rangle_\omega^\Omega, \tag{4}$$

where $\hat{\epsilon}^2 \equiv \left(\Omega_\star / \sqrt{\mathcal{G} M_\odot / R_\odot^3} \right)^2 = (\Omega_\star / \Omega_c^\odot)^2$ with $M_\odot$ and $R_\odot$ the mass and radius of the Sun, which allows us to express the variation of the radius of the star along time. The frequency-averaged dissipation provides us with a reasonable order of magnitude of the friction applied on tidal inertial waves in a rotating convective envelope as a function of its structural properties (radius and mass aspect ratios) and rotation rate. However, Ogilvie & Lin (2007) showed how the dissipation of these waves can vary over several orders of magnitude when inertial waves are excited. This may lead, for a given frequency, to strong differences with the frequency-averaged value. Taking into account such a complex frequency-dependence would require coupling coherently high-resolution hydrodynamical numerical simulations of tidal inertial waves to secular stellar evolution and orbital codes and to heavy computation procedures (e.g. Witte & Savonije 2002). Using, as a first step, frequency-averaged dissipation thus constitutes an intermediate and necessary step that allows us to explore a broad parameter space for planetary systems and their host stars.

2.1.3. Modified equivalent tidal quality factor

In a large number of studies on the tidal evolution of planetary systems, a quantity called the equivalent tidal quality factor is used (e.g. Goldreich & Soter 1966). This quantity comes from the modelling of the tidal response with an idealized system made of a harmonic oscillator (the forcing frequency corresponds to the excitation frequency imposed by the perturbing body and the Coriolis acceleration is the restoring force) and a damper (corresponding in this framework to a turbulent viscosity, see Greenberg 2009). Following Ogilvie & Lin (2007), the equivalent modified tidal quality factor $\overline{Q'}$ is introduced and expressed in terms of the tidal dissipation $\langle \mathcal{D} \rangle_\omega$ as

$$\overline{Q'} = \frac{3}{2 \langle \mathcal{D} \rangle_\omega} = \frac{3}{2} \frac{\overline{Q}}{k_2}. \tag{5}$$

In this equation, we also recall the usual expression as a function of the equivalent tidal quality factor $\overline{Q}$ and the second-order Love number k_2. For a homogeneous fluid body $k_2 = 3/2$ and $\overline{Q'} = \overline{Q}$. Using $\overline{Q'}$ allows us to avoid explicitly computing k_2. Indeed, we recall that the real physical quantity is the dissipation while its expression as a function of k_2 and $\overline{Q}$ comes from the simplified constant tidal quality factor model (e.g. MacDonald 1964). By definition, the lower the equivalent tidal quality factor, the more thermal energy is liberated into the star by the tidal dissipation process and the stronger the impact on the planet's orbit.

The modified equivalent tidal quality factor is usually considered as a free parameter to fit to a given star–planet system (Jackson et al. 2008; Ferraz-Mello et al. 2015). Moreover, this quantity is often assumed to be constant throughout the entire stellar evolution (e.g. Mardling & Lin 2002; Jackson et al. 2008; Ferraz-Mello et al. 2015), which leads to non realistic orbital evolution that cannot reproduce the

observed dearth of hot-Jupiter planets around rapidly rotating stars (Lanza & Shkolnik 2014; Teitler & Königl 2014; McQuillan et al. 2013; Mazeh et al. 2016).

Just as we could estimate the impact of the stellar structure on tidal dissipation (i.e. the tidal dissipation at a fixed rotation rate), we can define the equivalent structural quality factor as follows:

$$\overline{Q'}_s = \hat{\epsilon}^2 \overline{Q'} = \frac{3}{2} \frac{\hat{\epsilon}^2}{\langle \mathcal{D} \rangle_\omega} = \frac{3}{2} \frac{1}{\langle \hat{\mathcal{D}} \rangle_\omega^\Omega}. \tag{6}$$

2.1.4. Orbital evolution model

In order to compute the orbital evolution of close-in planets we use the model introduced in Bolmont & Mathis (2016). The evolution of the semi-major axis a of a planet on a circular orbit is given by (Hansen 2010; Leconte et al. 2010; Bolmont et al. 2011, 2012)

$$\frac{1}{a} \frac{da}{dt} = -\frac{1}{T_\star} \left[1 - \frac{\Omega_\star}{n} \right], \tag{7}$$

where n is the orbital frequency of the planet and $T_\star$ is an evolution dissipation timescale given by

$$T_\star = \frac{2}{9} \frac{M_\star}{M_p (M_p + M_\star)} \frac{a^8}{R_\star^5} \frac{\overline{Q'}_s}{\hat{\epsilon}^2} \frac{|n - \Omega_\star|}{\mathcal{G}}, \tag{8}$$

which depends on the semi-major axis a of the planet, the mass $M_\star$ and radius $R_\star$ of the star, the mass M_p of the planet, the stellar equivalent structural quality factor $\overline{Q'}_s$, and $\mathcal{G}$ the gravitational constant. Equation (8) shows that 1) the farther away the planet, the higher the evolution timescale; 2) the smaller the radius of the star, the higher the evolution timescale; and 3) the higher the quality factor $\overline{Q'}_s$, the higher the evolution timescale. We would like to point out here a typo in Bolmont & Mathis (2016), where a k_2 factor was forgotten in Eqs. (4) and (10)[1]. Despite the typo, however, the numerical results of Bolmont & Mathis (2016) are correct.

As in Bolmont et al. (2012) and Bolmont & Mathis (2016), we consider the influence of tides and of the stellar wind on the rotation of the star. The expression for the angular momentum loss rate is from the modified Kawaler (1988) braking law proposed in Bouvier et al. (1997),

$$\frac{1}{J} \frac{dJ}{dt} = \frac{-1}{J} K \Omega_\star^\mu \omega_{sat}^{3-\mu} \left(\frac{R_\star}{R_\odot} \right)^{1/2} \left(\frac{M_\star}{M_\odot} \right)^{-1/2} + \frac{1}{J} \frac{h}{2T_\star} \left[1 - \frac{\Omega_\star}{n} \right], \tag{9}$$

where J and h are the stellar and orbital angular momentum, respectively. The parameters K, μ, and ω_{sat} are wind parameters of the model from Bouvier et al. (1997). We refer the reader to Bolmont & Mathis (2016) for the values of these parameters. We also recall that the braking law used in this orbital evolution model is somewhat outmoded compared to the recent theoretical advances in this field (see Matt et al. 2015; Réville et al. 2015). While including a more realistic braking law will not affect the general conclusion of this work, it could lead to small deviation in a given orbital evolution. Conversely, and since the star is considered a solid body in this work, including the core-envelope decoupling in the model will lead to very distinct orbital evolution. In this framework, we are now investigating the effect of

---

[1] Equation (4) in Bolmont & Mathis (2016) is $k_2 / \overline{Q} = \sin[2\delta]$, but it should be $k_2 / \overline{Q} = k_2 \sin[2\delta]$ (Remus et al. 2012). This leads to $\Delta \tau_\star = \frac{3}{4 k_2 \overline{Q'} |n - \Omega_\star|}$.
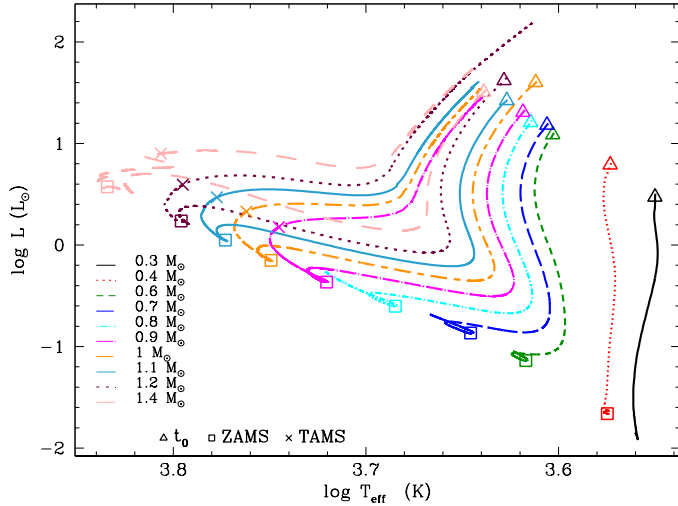
Fig. 1. Stellar evolution tracks in the Hertzsprung-Russell diagram for the rotating models of 0.3, 0.4, 0.6, 0.7, 0.8, 0.9, 1.0, 1.1, 1.2, and 1.4 $M_\odot$ at solar metallicity. We show the evolution up to the RGB for the more massive stars or up to the evolution stage the models reach at 20 Gyr for the less massive stars. Legend: the first step in each evolution sequence (triangle), the ZAMS (square), and the TAMS (cross).

Table 1. Phases and ages reached by our models at the end of each of the simulations.

$M_\star$	Phase	Age
0.3 $M_\odot$	PMS	30.21 Gyr
0.4 $M_\odot$	MS	20.17 Gyr
0.6 $M_\odot$	MS	19.98 Gyr
0.7 $M_\odot$	MS	20.49 Gyr
0.8 $M_\odot$	MS	19.99 Gyr
0.9 $M_\odot$	RGB	19.29 Gyr
1.0 $M_\odot$	RGB	13.05 Gyr
1.1 $M_\odot$	RGB	9.12 Gyr
1.2 $M_\odot$	RGB	6.59 Gyr
1.4 $M_\odot$	RGB	3.73 Gyr

a more realistic rotational evolution on the orbital evolution of close-in planets, which will be presented in a forthcoming paper.

When the dynamical tide is driving the evolution, the structural equivalent tidal quality factor ($\overline{Q'_s}$) is given by Eq. (6). When the equilibrium tide is driving the evolution, we use the observational constraints of Hansen (2012), which are given in terms of a constant normalized tidal dissipation factor $\overline{\sigma_\star}$, depending on the stellar mass. We refer to Bolmont & Mathis (2016) for the correspondence between the tidal quality factor and the tidal dissipation factor $\overline{\sigma_\star}$. For instance, the normalized dissipation factor for a 1.0 $M_\odot$ star is taken to be $\overline{\sigma_\star} = 3 \times 10^{-7}$; for a 1.2 $M_\odot$ star it is $\overline{\sigma_\star} = 7.8 \times 10^{-8}$. We recall that assuming a constant dissipation of the equilibrium tide constitutes a simplified model, which should be improved in the near future. Indeed, as explained in the introduction, it varies along the evolution of stars (e.g. Zahn & Bouchet 1989; Villaver & Livio 2009; Mathis et al. 2016).

While the work of Mathis (2015) provides a realistic evaluation of the evolution of the tidal dissipation for low-mass stars from the PMS to the subgiant (SG) phase, it was done at fixed stellar rotation along the evolution. Here we go one step further and treat rotation evolution coherently in STAREVOL. This allows us to follow the impact of rotation on the stellar structure and evolution tracks, and to study self-consistently the dissipation of the tidal waves inside the convective envelope of rotating stars over a wider range of evolutionary phases.

2.2. Models of low-mass stars including rotation

This study is based on a grid of stellar models of rotating stars we computed with the code STAREVOL (see e.g. Amard et al. 2016) for a range of initial masses between 0.3 and 1.4 $M_\odot$ at solar metallicity ($Z = 0.0134$; Asplund et al. 2009). Figure 1 shows the stellar evolution tracks of these models in the Hertzsprung-Russell diagram. Table 1 summarizes at which evolutionary step the models in this work stop.

The references for the basic input microphysics (equation of state, nuclear reactions, and opacities) can be found in

Amard et al. (2016) and in Lagarde et al. (2012). The initial helium abundance and mixing length parameter are calibrated without atomic diffusion to reproduce a non-rotating Sun with respect to the solar mixture of Asplund et al. (2009) with a 10^{-5} precision for the luminosity and the radius at the age of the Sun. The corresponding mixing length parameter and initial helium abundance are $\alpha_{\rm MLT} = 1.6267$ and $Y = 0.2689$.

The stellar evolution models are computed taking into account rotation:

– The evolution of angular momentum in the stellar interior is calculated from the first iteration step on the PMS phase up to the RGB following the formalism developed by Zahn (1992), Maeder & Zahn (1998), and Mathis & Zahn (2004). This formalism takes into account advection by meridional circulation and diffusion by shear turbulence (see Palacios et al. 2003, 2006; Decressin et al. 2009). The internal transport prescriptions used to describe turbulent diffusion coefficients are Mathis et al. (2004) in the horizontal direction and Talon & Zahn (1997) in the vertical direction.
– The convective region is assumed to be in solid-body rotation and is subject to magnetic braking from the PMS onward and up to the RGB following the Matt et al. (2015) prescription. The mass loss rate is estimated using the prescription of Cranmer & Saar (2011).
– Star–disc interaction is taken into account during the early-PMS phase (i.e. during the first 2 to 10 Myr). Following Gallet & Bouvier (2015), the surface rotation rate is assumed to be held constant during a characteristic timescale (the disc's lifetime). This phase is considered an initial condition for angular momentum evolution and is fixed by the observations (see Gallet & Bouvier 2015).
– The initial stellar rotation is fixed using the calibration for fast rotators from Gallet & Bouvier (2015): an initial rotation period of 1.4 days (corresponding to $\Omega_\star = 18\ \Omega_\odot$) and a disc lifetime of 3 Myr corresponding to the calibration of the solar-type stars. We applied this parameterization to the whole range of masses (0.3 to 1.4 $M_\odot$) to analyse the impact of the stellar mass on the evolution of the dissipation. To reproduce the observed distribution of surface rotation period in star-forming regions and young-open clusters, we should have calibrated the initial conditions for each stellar mass (Gallet & Bouvier 2013, 2015; Amard et al. 2016). However, this calibration is beyond the scope of the present study, where we perform a wide exploration of the parameter space.

Figure 2 shows the evolution as a function of time of the main stellar quantities that enter in the expression of the equivalent
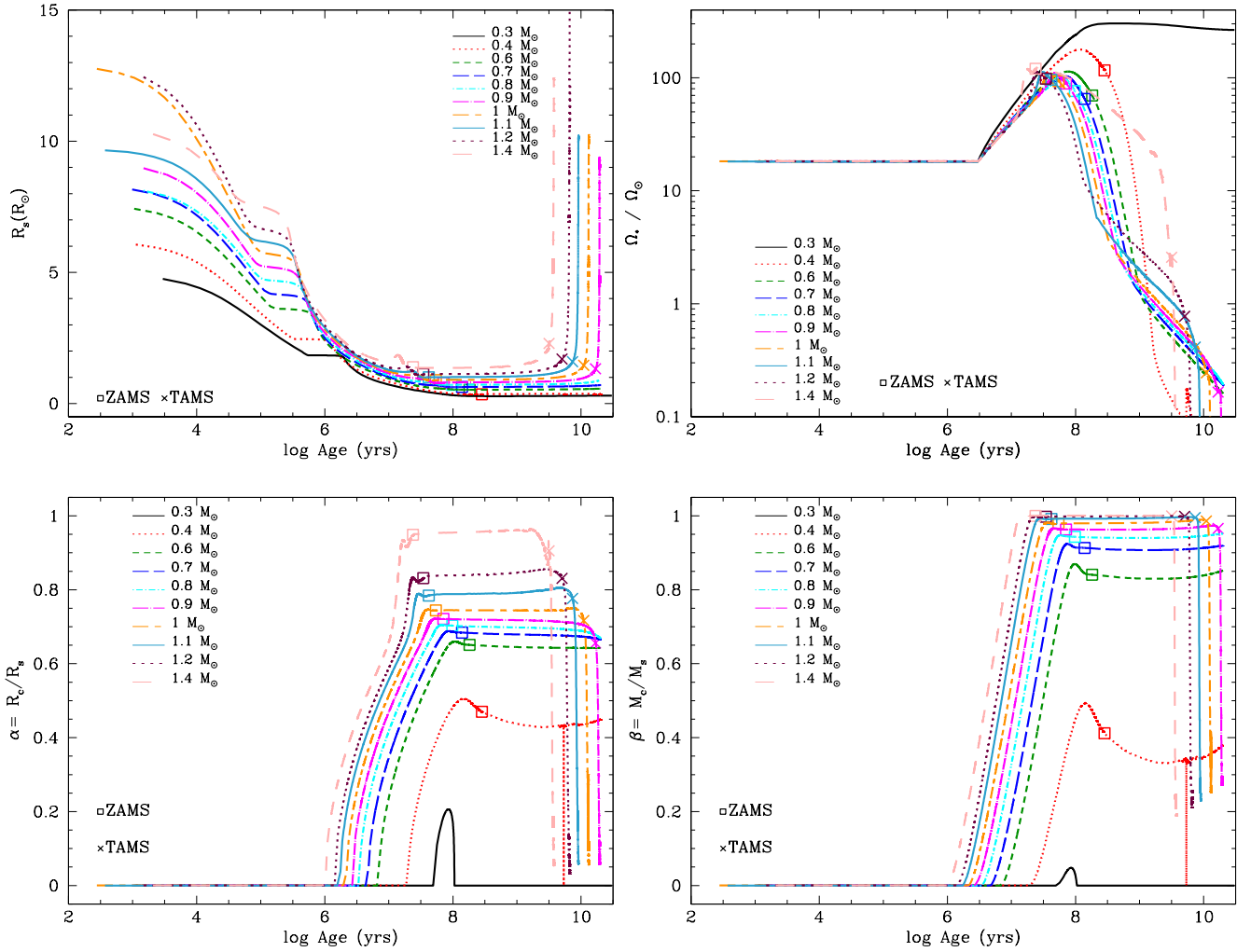
Fig. 2. *Top left*: evolution of the stellar radius $R_\star$ of stars from 0.3 to 1.4 $M_\odot$ as a function of time. *Top right*: surface angular velocity evolution (scaled to the present Sun angular velocity $\Omega_\odot = 2.87 \times 10^{-6}$ s^{-1}) for the different stellar masses. *Bottom left*: evolution of the radius aspect ratio $\alpha = R_c/R_\star$ of stars from 0.3 to 1.4 $M_\odot$ as a function of time. *Bottom right*: evolution of the mass aspect ratio $\beta = M_c/M_\star$ of stars from 0.3 and 1.4 $M_\odot$ as a function of time. Legend: the first step in each model (triangle), the ZAMS (square), and the TAMS (cross). Table 1 summarizes at which evolutionary step the models in this work stop.

tidal quality factor, namely the stellar radius ($R_\star$), the surface angular velocity ($\Omega_\star$), the radius aspect ratio $\alpha = R_c/R_\star$, and the mass aspect ratio $\beta = M_c/M_\star$. This is shown for all the stellar masses considered in the computations.

We note that our stellar evolution and orbital evolution models are not strictly coupled. Grids of structural quality factor $\overline{Q'_s}$ are initially computed using STAREVOL for stars with an initial rotation period of 1.4 days and later provided to the orbital evolution code of Bolmont et al. (2012), with which we compute the rotational evolution of the stars including the tidal torque and the torque produced by the stellar winds (see Eq. (9)).

3. Tidal dissipation along the evolution of rotating stars

As described by Eq. (1), the frequency-averaged tidal dissipation intrinsically follows the evolution of both the internal structure (through the α and β parameters and $R_\star$) and the rotation rate (through the ϵ parameter) of the star. Here we investigate successively the effect of the evolution on the stellar structure (Sect. 3.1) and the effect of the rotation rate (Sect. 3.2) on the

evolution of the frequency-averaged tidal dissipation and the equivalent modified quality factor.

3.1. Structural effect: evolution paths in the (α, β) plane

To analyse how the dissipation evolves with the stellar structure, we first consider the frequency-averaged dissipation at fixed normalized angular velocity, as in Mathis (2015)[2]. Figure 3 shows the intensity of the frequency-averaged dissipation at fixed normalized angular velocity ($\langle \mathcal{D} \rangle_\omega^\Omega$) as a function of both mass and radius aspect ratios (α and β) (colour-coded gradient). The right-hand lower white region in Fig. 3 is excluded as it is the non-physical (α, β) area where the condition $\gamma < 1$ (i.e. the core denser than the envelope) is not fulfilled. The value of $\langle \mathcal{D} \rangle_\omega^\Omega$ exhibits a maximum in an island region around

---

[2] The evolution models of Siess et al. (2000) used by Mathis (2015) were computed without rotation. However, in the case of low-mass stars, rotation has only a very modest effect on the stellar tracks (effective temperature and luminosity) and on the stellar structure (aspect ratios). We thus expect to find behaviours that are very similar to the Mathis (2015) predictions.
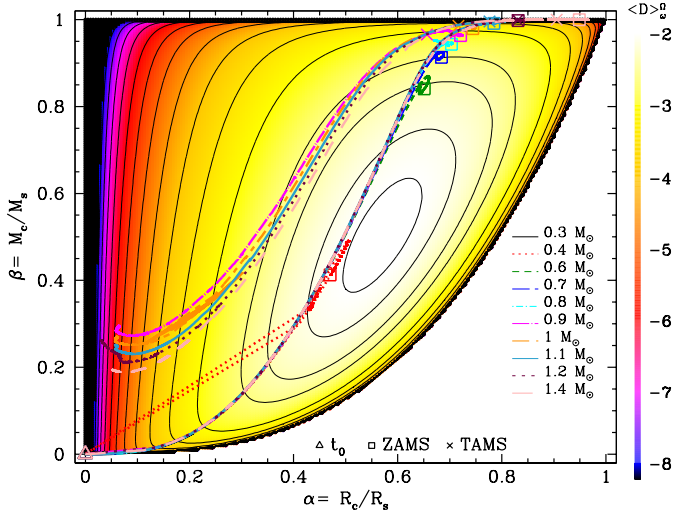
Fig. 3. Variation of normalized dissipation $\langle\mathcal{D}\rangle_\omega^\Omega$ as a function of the radius and mass aspect ratios (α and β, respectively) in colour scale. Levels are for $\log\langle\mathcal{D}\rangle_\omega^\Omega = \{-2, -2.1, -2.3, -2.5, -3, -3.5, -4, -4.5, -5, -5.5, -6, -6.5, -7, -7.5,$ and $-8\}$. The evolutionary paths of the stellar models of the different masses (see labels) are overplotted in the (α, β) plane. Symbols are the same as in Fig. 1.

($\alpha_{max} = 0.572$, $\beta_{max} = 0.503$) corresponding to an intensity of 1.091×10^{-2}. We note that the regimes where stars are almost fully convective correspond to regular inertial waves for which dissipation is weak (Wu 2005, in black and dark blue), while when the radiative core is sufficiently extended sheared wave attractors with strong dissipation can form (Ogilvie & Lin 2007, yellow to white).

The interest is then to overplot in the (α, β) parameter space the evolution tracks of our stellar models (including rotation, but see footnote 2) and to describe their behaviour at each evolutionary phase.

PMS-ZAMS

Since all the models start their evolution with a fully convective interior, α and β are initially equal to zero. Then both aspect ratios increase as the star contracts and the radiative core develops during the PMS up to the zero-age main sequence (ZAMS). As a consequence, the general behaviour of the tidal dissipation shown in Fig. 3 can be easily understood. As both mass and radius aspect ratios of the models increase along the PMS, the stars successively pass through regions of increasing intensity until they brush against the islet of maximum intensity (surrounded by the level $\log\langle\mathcal{D}\rangle_\omega^\Omega = -2$, see Fig. 3). According to Fig. 2, the stars with masses higher than 0.3 $M_\odot$ reach this islet on a short timescale between 3 Myr (1.4 $M_\odot$) and 100 Myr (0.4 $M_\odot$). Then they move away from this maximum intensity region as both mass and radius aspect ratios continue to increase while the stars approach the ZAMS. Just before the ZAMS, several reactions have already been initiated, such as the p-p chain and the CN reaction, which produce enough energy to stop the stellar contraction. The more massive stars then develop a convective core, while their effective temperature and luminosity slightly decrease as they settle on the ZAMS. This affects the whole radius of the star, explaining the "bump" that is clearly visible in Fig. 1 for all the quantities, and inducing a sharp increase of the dissipation. This increase is not visible in Fig. 3, but clearly

visible in the left panels of Fig. 4 for the highest mass star. The case of the 0.3 $M_\odot$ star is quite interesting because it hosts a very small radiative core during a very brief moment ($\Delta t = 50$ Myr) before reaching the ZAMS. This stellar mass represents the limit between fully convective and partly radiative stars. As pointed out before, the dynamical tide induced dissipation is lower for fully convective stars because the tidal waves that propagate through the convective envelope of the star require the presence of a radiative core on which they can reflect to lead to an important dissipation. This effect is highlighted by Eq. (1), which shows that the dissipation strongly depends on the mass and radius aspect ratio of the radiative core of the star. Since these ratios are equal to zero in fully convective stars, compared to partly convective stars, fully convective stars are then less dissipative.

ZAMS-TAMS

Even though the stars stay on the main sequence (MS) for about 90% of their life, their path in Fig. 3 evolves very little during that phase, and remains in the low tidal dissipation region (upper black era) with an almost constant frequency-averaged tidal dissipation. This occurs because the stellar radius and internal structure (thus α and β) evolve only modestly along the MS. Close to the terminal-age main sequence (TAMS; crosses in Fig. 2) the stellar radius starts to increase more rapidly without noticeable change in the mass of the convective envelope, which induces a decrease in α at almost constant β.

Evolved phase

As the stars evolve along the SG towards low effective temperatures, the stellar radius increases and the convective envelope deepens in both mass and radius. This explains the sharp and rapid decrease in both the mass and radius aspect ratios α and β (Figs. 2 and 3). At the end of the first dredge-up on the RGB, the convective envelope recedes again in mass, and β slightly increases again. Consequently, during the SG and RGB phase the evolution tracks in the (α, β) plane pass again through regions of higher dissipation (up to an intensity of $\log\langle\mathcal{D}\rangle_\omega^\Omega = -2.5$) before heading in the region of very low dissipation towards the RGB when the stellar radiative core is very small in both mass and radius.

Summary: Hysteresis-like cycle along the evolution

In Fig. 3 we clearly see the evolutionary path followed by low-mass stars in the (α, β) plane as well as the resulting evolution of the tidal dissipation intensity (at fixed rotation). All the solar-metallicity models with masses between 0.3 and 1.4 $M_\odot$ develop a radiative core and follow an hysteresis-like cycle: the tidal dissipation intensity is first very low, then it increases and reaches a maximum value during the PMS phase before decreasing again at the arrival on the ZAMS; it stays almost constant along the MS, and increases again during the first dredge-up phase on the SG and at the base of RGB before decreasing in the upper part of the RGB. As expected, we confirm the results of Mathis (2015) and extend the predictions towards more advanced evolution phases.

3.2. Rotational effect: dissipation and equivalent modified quality factor as a function of time and effective temperature

We explore now the effects of the variations of the stellar rotation rate along the evolution on the dissipation and equivalent
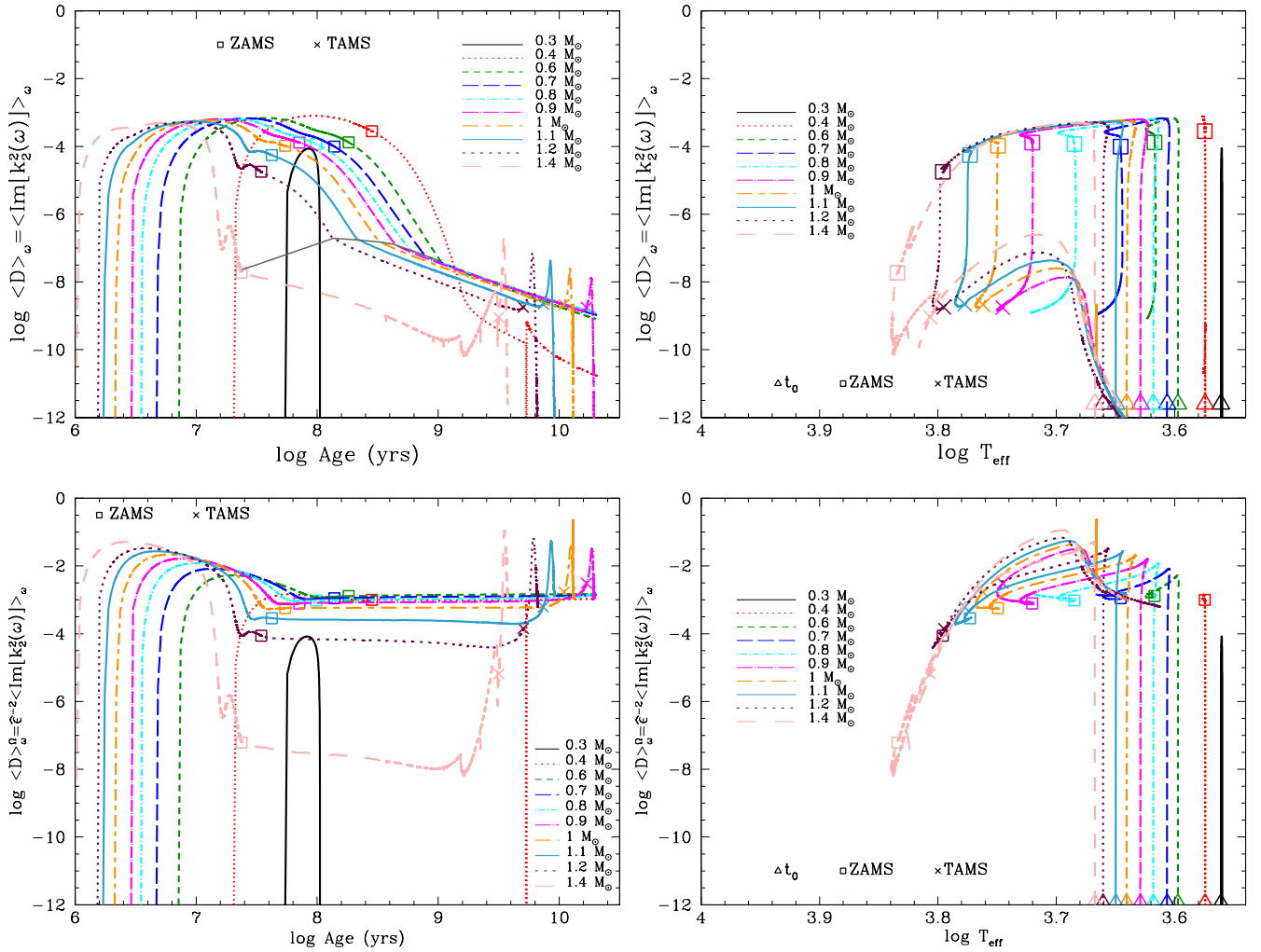
Fig. 4. *Upper panels*: evolution of the frequency-averaged tidal dissipation $\langle \mathcal{D} \rangle_\omega = \langle \mathrm{Im}\left[k_2^2(\omega)\right]\rangle_\omega$, as a function of time (*left*) and effective temperature (*right*) for stellar masses ($M_\star$) from 0.3 to 1.4 $M_\odot$. *Lower panels*: same as the upper panels, but at a fixed normalized angular velocity $\langle \hat{\mathcal{D}} \rangle_\omega^\Omega = \hat{\epsilon}^{-2}\langle \mathrm{Im}\left[k_2^2(\omega)\right]\rangle_\omega$.

modified quality factor. As described in Sect. 2.2, the surface velocity of our stellar models evolves under the action of the secular variations (expansion and contraction), of magnetic braking, and of internal transport processes. We refer to Amard et al. (2016) for details. What matters for the present study are the general trends. After a few Myrs on the PMS, a star is disconnected from its disc, it spins up as its stellar radius decreases up to the ZAMS. On the MS, the surface rotation decreases continuously because of the wind braking. After the TAMS, the expansion of the stellar radius leads to the continuous decrease of the stellar angular velocity until the star reaches the tip of the RGB.

Figures 4 and 5 show the evolution of the frequency-averaged tidal dissipation and its corresponding equivalent quality factor, respectively. In each of these figures, the upper panels display the full dissipation/equivalent quality factor including structural and rotational evolution effects; for comparison, the lower panels display its normalized version (here normalized to the sun's critical ratio $\hat{\epsilon}$, see Eqs. (4) and (6)) where rotational effects are filtered out. The left panels of Figs. 4 and 5 display the tidal dissipation and equivalent quality factor as a function of time, while the right panels show these quantities as a function of the effective temperature (which is a more physical quantity compared to age). We note that the lower panels of our

Fig. 4 provide us with the results obtained in Fig. 4 of Mathis (2015) on the PMS and the MS.

The evolution of the normalized tidal dissipation follows the evolution of the internal structure of the star. In the lower left panel of Fig. 4 we retrieve the different regimes followed by the frequency averaged tidal dissipation intensity at fixed rotation as described in Sect. 3.1. This structural modulation is also found, but inverted, in the evolution of the equivalent structural quality factor as a function of time (see lower left panel of Fig. 5). The main effects of relaxing the normalization on the rotation rate are that the tidal dissipation is lower (on the PMS) by about two orders of magnitude toward lower intensity as $\epsilon \ll 1$, and that the behaviour of the dissipation (on the MS) is drastically changed (see Figs. 4 and 5) because of stellar spin-down driven by magnetized winds.

Even if the rotation rate is evolving during the PMS phase (see upper right panel of Fig. 2) it has no impact on the behaviour of the tidal dissipation (or equivalent quality factor) since the rotation itself is entirely controlled by the stellar contraction (i.e. by the internal structure). During the Hayashi phase, as the star contracts and its core develops, the tidal dissipation (equivalent quality factor) first increases (decreases) at almost constant effective temperature (see right panels of Figs. 4 and 5). Then
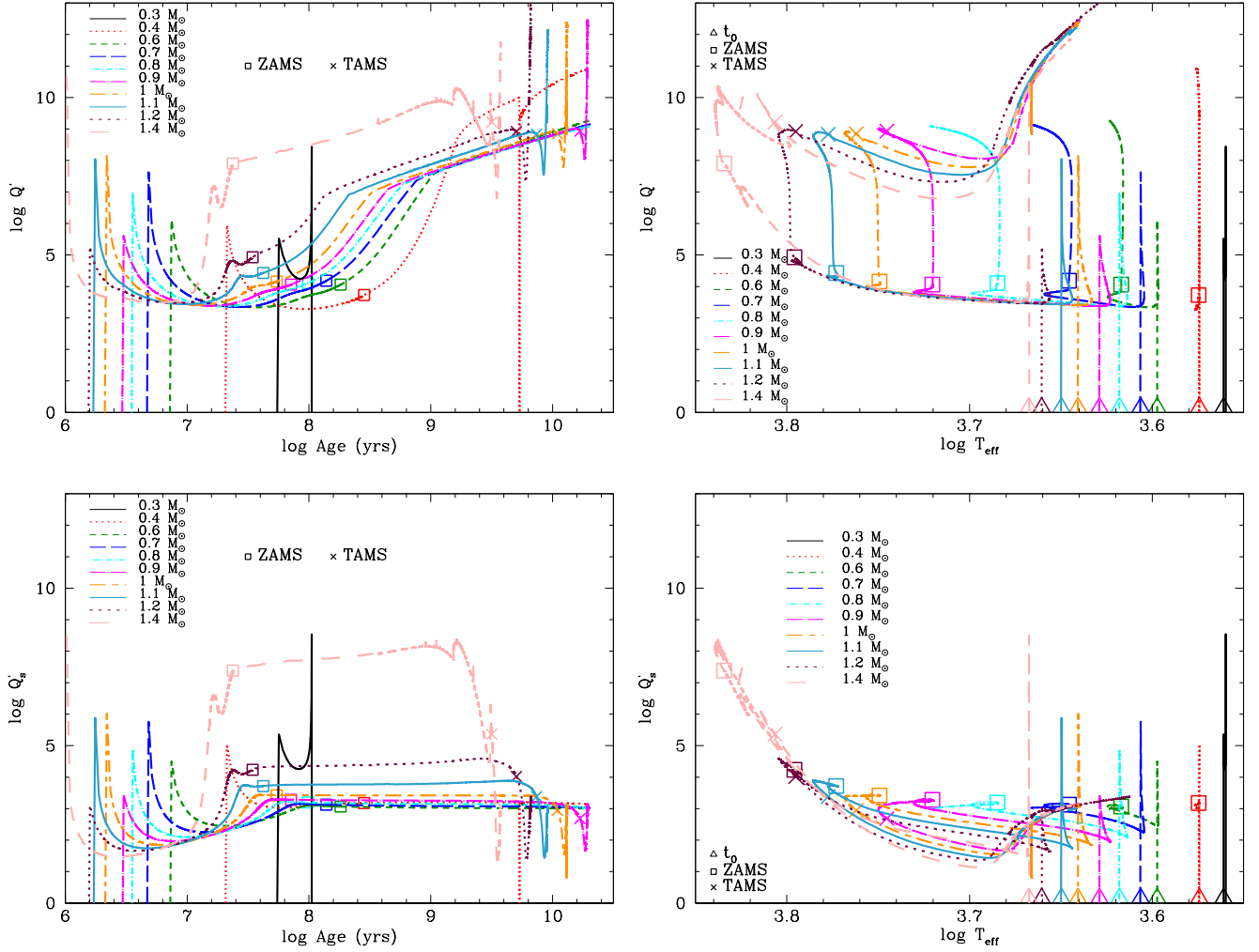
Fig. 5. *Upper panels*: equivalent modified tidal quality factor $\overline{Q'} = 3/(2\langle\hat{\mathcal{D}}\rangle_\omega)$ as a function of time (*left*) and effective temperature (*right*). *Lower panels*: equivalent structural modified quality factor $\overline{Q'}_s = 3/(2\langle\hat{\mathcal{D}}\rangle_\omega^\Omega)$ as a function of time (*left*) and effective temperature (*right*).

on the Henyey phase, the dissipation (equivalent quality factor) reaches a plateau while the effective temperature slightly decreases. Just before the ZAMS, the dissipation (equivalent quality factor) decreases (increases) as the star slightly expands.

During the MS phase, and as pointed out above, both the mass and radius aspect ratios remain more or less constant. At this point, the internal structure stops controlling the evolution of the tidal dissipation (equivalent quality factor). From the ZAMS and up to the TAMS, the tidal dissipation (equivalent quality factor) is controlled by the evolution of the surface angular velocity and thus by the extraction of angular momentum (see Sect. 2.2). As a consequence, the tidal dissipation (equivalent quality factor) continuously decreases (increases) towards the TAMS. We note the stall in this evolution that is due to the transition between saturated and unsaturated wind regime (see Matt et al. 2015, and references therein, and the grey line in the upper left panel of Fig. 4). Indeed, this stall in almost all rotational tracks is due to a change in saturation regime induced by the saturation of the magnetic field that observationally appears around Ro = 0.1 (Saar 1996, 2001; Reiners & Mohanty 2012). The effect of this magnetic saturation is to reduce the efficiency of the braking law (see Kawaler 1988). During this phase, while the temperature decreases, the tidal dissipation (equivalent quality factor) linearly in logarithmic scales decreases (increases) at almost constant effective temperature.

Finally, after the TAMS and along the SG and RGB phases, the dissipation (equivalent quality factor) first starts to increase (decrease) as both mass and radius aspect ratio move closer to the island of maximum intensity (see Fig. 3), and then decreases (increases) as both aspect ratios are strongly reduced by the stellar expansion, leading to structure closer to weakly dissipative fully convective stars.

The tidal dissipation and equivalent quality factor are thus strongly affected by the variations of the rotation rate along the evolution of the star. The parameter $\overline{Q'}$ reaches maximum values up to 10^{12} (for the more massive stars in our sample) from 10^6 to 10^{10} yr, while $\overline{Q'}_s$ reaches maximum values up to 10^8 during the same period. Compared to the case of fixed angular velocity (Sect. 3.1 and Mathis 2015) the variations of rotation along the evolution lowers the values of the equivalent quality factor and tidal dissipation by four orders of magnitude. This is especially true on the MS when the structure $(\alpha, \beta, R_\star)$ is almost fixed but the rotation rate evolves (decreases) significantly.

The right panels of Figs. 4 and 5 also show the hysteresis cycle followed by the higher mass stars considered here. From the earliest steps of the PMS phase up to the RGB, the tidal dissipation almost achieves a loop by nearly reaching its initial starting point. We note that this hysteresis cycle, which is clearly visible in the case of the normalized tidal dissipation, is not as
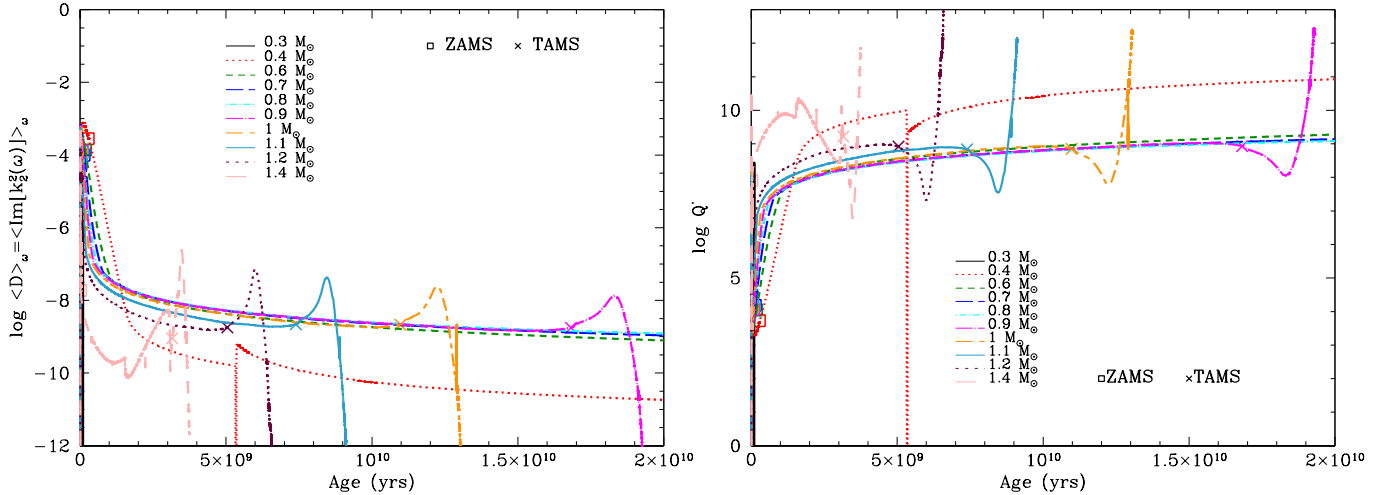
Fig. 6. Frequency-averaged tidal dissipation $\langle \hat{\mathcal{D}} \rangle_\omega$ (*left*) and equivalent modified tidal quality factor $\overline{Q'} = 3/(2\langle \hat{\mathcal{D}} \rangle_\omega)$ (*right*) as a function of time in linear scale. Legend: the ZAMS (square) and the TAMS (cross).

pronounced in the case of the non-normalized dissipation because of the action of rotation.

4. Orbital evolution during evolved stellar phase

We showed in Sect. 3 that the tidal dissipation $\langle \mathcal{D} \rangle_\omega$ (or the equivalent tidal quality factor $\overline{Q'}$) strongly varies from the PMS to the RGB along with the structural parameters and rotation rate of the star[3]. These variations of several orders of magnitude should have an impact on the tidal evolution of close-in planets. We investigate here the effect of the tidal dissipation evolution during the evolved stellar phases on the orbital evolution of a 1 $M_{\rm jup}$ mass planet. The other phases of tidal evolution have been intensively investigated in Bolmont & Mathis (2016). In particular, the high dissipation occurring during the PMS phase is responsible for important planetary migration. Indeed, by including the frequency-averaged dynamical tide formalism of Mathis (2015) and Ogilvie (2013) in an orbital evolution code, Bolmont & Mathis (2016) pointed out strong outward migration of close-in planets outside the stellar co-rotation radius and inward migration (where the planet eventually falls into the star) for close-in planet initially inside of the co-rotation radius. With this work, they completely change the conclusion of Bolmont et al. (2012) who only used the equilibrium tide formalism.

The evolved phases correspond here to the SG phase and RGB phase, which are represented in Fig. 1. The evolutionary tracks can be divided into two parts: the SG phase occurring just after the TAMS (cross symbol in Fig. 1), which is characterized by an almost constant luminosity and a decrease in effective temperature, and the RGB phase, which is characterized by an increase in luminosity and a decrease in effective temperature. Figure 6 shows the evolution of the tidal dissipation (left) and equivalent quality factor (right) as a function of time in linear scale for these two late phases.

---

[3] Our tidal orbital evolution models are not now strictly coupled to the stellar evolution models. We use grids for the structural tidal dissipation $\overline{Q'}_{\rm s}$ which come from grids of $\overline{Q'}$ calculated for an initial rotation period of 1.4 days. We then compute ϵ to recover a consistent $\overline{Q'}$ from the evolution of the stellar rotation given by the equations of Bolmont et al. (2012) and Bolmont & Mathis (2016).

At the end of the MS phase, there is no more hydrogen in the core and the helium core is then deprived of nuclear sources and contracts. The stellar core becomes isothermal (the temperature is insufficient to burn helium) and contracts. Hydrogen burning then migrates into a shell around the helium core. The combination of core contraction and shell hydrogen burning leads to an expansion of the stellar radius and to an inflation of the envelope. The SG phase corresponds more precisely to a decrease in the effective temperature at almost constant luminosity, which is a direct consequence of the convective envelope expansion and the core contraction. The tidal dissipation therefore increases during a short phase as the mass and radius aspect ratio of the radiative core decreases toward lower values and the star crosses again the (α, β) plane from top right to bottom left. However, once the maximum is reached, the dissipation sharply decreases close to zero. It results in a "bump" seen in Figs. 4 and 5 between 3 Gyr (1.4 $M_\odot$) and 20 Gyr (0.9 $M_\odot$). The underlying idea is to know whether this bump has an impact on the evolution of the semi-major axis of a Jupiter-mass planet or not.

Figure 7 shows the evolution of the semi-major axis of a 1 $M_{\rm jup}$ planet orbiting a 1 $M_\odot$ star with an initial rotation period of 1 day. The orbital evolutions were computed using Eqs. (7) and (8) (see Sect. 2.1.4 and Bolmont & Mathis 2016, for more details). In contrast to previous models that did not take into account the contribution of the dynamical tide, this model allows a more complete picture of the stellar dissipation. We again note that the rotational evolution of the stars is estimated using the braking law from Bouvier et al. (1997). Even if the parametrization of the Bouvier et al. (1997) braking law is theoretically only valid for stars between 0.5 and 1.1 $M_\odot$, in our model the rotational evolution of the 1.2 $M_\odot$ star is consistent with the expected behaviour of a 1.0 and 1.1 $M_\odot$ star (see Gallet & Bouvier 2015; Amard et al. 2016) with a surface rotation rate that reaches a 10-day period between 1 and 2 Gyr.

Figure 7 (left and right) shows that this bump has no effect on the evolution of the semi-major axis of the planets. There are two main reasons for this behaviour. The first is that planets susceptible to experiencing this bump in dissipation are located too far away for tides to impact them significantly. Indeed, they have to be in the region in which they excite the inertial waves in the convective envelope (i.e. where $P_{\rm orb} \rangle 1/2 P_\star$, $P_{\rm orb}$ is the orbital period of the planet, and $P_\star$ is the rotation period of the
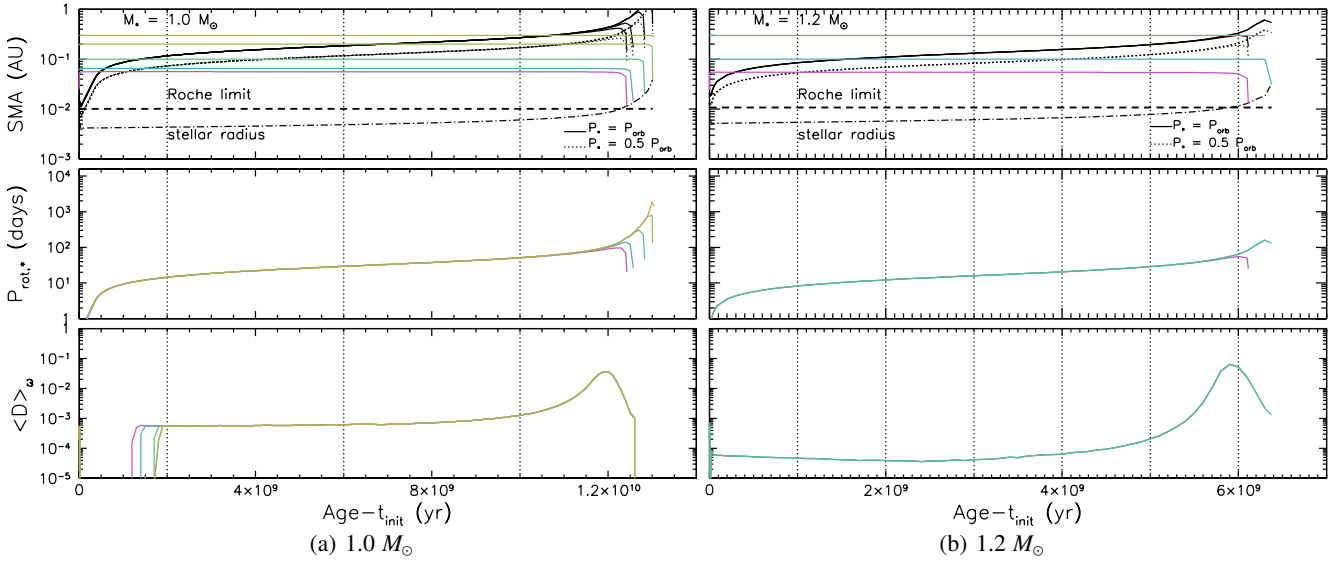
Fig. 7. Evolution of the orbital distance of a Jupiter mass planet with different initial semi-major axis (*top panel*), the stellar rotation period (*middle panel*) and the stellar dissipation factor (*bottom panel*) during the evolved phases (sub-giant and early RGB) of a 1.0 $M_\odot$ (*left*) and 1.2 $M_\odot$ (*right*) star. *Top panel*: the orbital distance of the planet is represented in full coloured lines. The full black lines correspond to the co-rotation distance ($P_{orb} = P_\star$), and the dotted black lines to $P_{orb} = 0.5\,P_\star$ delimiting the region where the dynamical tide operates. The long dashed black line corresponds to the Roche limit and the dashed-dotted line to the stellar radius. *Middle panel*: the surface rotation period (in days) of the host star. *Bottom panel*: the stellar dissipation $\langle \mathcal{D} \rangle_\omega$. The time on the *x*-axis is given from an initial time t_{init}, which corresponds to the time of the protoplanetary disc dispersal. This initial time is taken to be 5 Myr.

star) at the moment of the bump. The very close-in planets cross the limit $P_{orb} = 1/2P_\star$ too early in the evolution of the system. Only planets farther away than ~0.3 AU are still in the dynamical tide region at the time of the bump. The second reason is that the star has slowed down so significantly that at the age of the bump (around 12 Gyr for 1 $M_\odot$ and 6 Gyr for 1.2 $M_\odot$), its rotation is very slow (period of the order of 100 days). Mathis (2015), Bolmont & Mathis (2016), and Fig. 6 show that the dissipation in the star decreases as the star spins down, so that at the age of the bump the dissipation is actually very low and does not impact the orbital evolution of the planet. Figure 7 (left) shows that due to the stellar spin down, the bump is actually not visible. However, Fig. 7 (right) shows that for 1.2 $M_\odot$ the bump is visible.

Figure 7 (left and right) also show that when falling onto the expanding star the planets make it accelerate significantly. For instance, we find that a planet at 0.05 AU at 4.5 Gyr, induces a decrease in the rotation period from ~180 days (the value it would have without planets) to 20 days. This corresponds to an increase in surface velocity from 0.68 km s^{-1} to 6 km s^{-1}. Privitera et al. (2016b) also studied the influence of planet engulfment on stellar spin up for stars and find the same type of behaviour. However, their study was focused on higher mass stars (>1.5 $M_\odot$) and even later stages than in this work. They also took into account the mass loss from the star and the head wind planets feel due to the ejected matter. We did not take into account these phenomena because the mass loss for the stellar mass range and the phase we consider is not as important as for the objects they study.

We consider here Jupiter-like planets; however, this model could be used to investigate the future of the Earth as the Sun expands (as was done in e.g. Schröder & Connon Smith 2008). Nevertheless, the computed evolutionary models do not go to sufficiently advanced phases for such a small-mass planet at 1 AU to be impacted, and here we do not take into account the effect of the mass loss from the star on the orbital evolution of the

planets, which begins to be important at more advanced stages and which has a non-negligible effect on the orbital distances of planets. Here, our 1 $M_\odot$ model stops on the RGB at an age of 13 Gyr when the radius of the star is about 0.04 AU. Figure 7 (left) shows that even a Jupiter-mass planet at 0.3 AU is only just starting to be influenced by the tides at that age. This has two consequences: 1) when an Earth-mass planet can be influenced by the stellar tide (when the radius is large enough, see Eq. (8)), the star has spun down enough so that the planet would not evolve because of the dynamical tide but because of the equilibrium tide; and 2) even if the planet evolved due to the dynamical tide, the structure of the star would be such that the dynamic tide would be very weak (due to the huge size of the convective envelope). We would therefore not expect our model to change the predictions for the future of the Earth as the Sun becomes a red giant.

5. Conclusion

We extend the analysis of Mathis (2015) of the evolution of the dissipation of tidal inertial waves propagating in the convective envelope of low-mass stars from the PMS to the RGB tip. We take into account for the first time the variations of both stellar rotation and internal structure. As a first step, we assumed for the tidal dissipation model a simplified bi-layer stellar structure where the radiative core and the convective envelope have averaged densities. This allows us to obtain an analytical expression for the frequency-averaged tidal dissipation, which provides us with a reasonable order of magnitude of the dissipation in stellar convective envelopes as a function of their depth, mass, and rotation. In forthcoming works, the strong frequency-dependence of the dissipation of tidal inertial waves (Ogilvie & Lin 2007) and the radial variation of the density, which could both affect the strength of tidal friction should be taken into account. However, numerical modelling will become more complex and heavy. Our

approach thus constitutes a first and necessary step to explore a broad parameter space for planetary systems and their host stars. We use these new predictions for tidal dissipation to generalize the work of Bolmont & Mathis (2016); we follow in particular the orbital evolution of close in planets during advanced stages of stellar evolution.

By coupling the stellar evolution code STAREVOL to the frequency-averaged tidal dissipation and equivalent modified tidal quality factor prescription of Mathis (2015) and Ogilvie (2013), we have shown in this work that stellar evolution is crucial in tidal interaction modelling. Indeed, both the stellar structural evolution (through the presence of a radiative core, which can enhance the tidal excitation of inertial waves, e.g. Ogilvie & Lin 2007), and rotational evolution (through the scaling in ϵ^2 of the dissipation) strongly affect the evolution of the tidal dissipation and the corresponding equivalent tidal quality factor.

While the evolution of the stellar structure controls the evolution of the dissipation during the PMS phase, rotation governs its evolution during the MS phase. Indeed, during the PMS phase the rotation itself is restrained by the evolution of the internal structure through the stellar contraction, while during the MS phase, the internal structure remains more or less constant leaving room for a rotational modulation of the dissipation via the wind braking mechanism.

Thanks to the coupling between STAREVOL and the frequency-averaged tidal dissipation prescription, we can provide the community with an online tool[4] that will provide tidal dissipation and the equivalent quality factor evolution for each stellar mass considered in this work.

This grid can be used to better constrain models dedicated to the study of the orbital evolution of planetary systems. More specifically it can be used by ongoing and past space missions such as CoRoT and *Kepler*/K2 (CoRot Team 2016; Borucki et al. 2010; Howell et al. 2014) and by future space and ground-based observatories such as CHEOPS (Broeg et al. 2015), TESS (Ricker et al. 2015), PLATO (Rauer et al. 2014), and SPIRou (Moutou et al. 2015).

In this paper, and based on the work of Bolmont & Mathis (2016), we explored the orbital evolution of close-in planets during evolved stellar phases (namely the RGB). Using the new predictions of tidal dissipation for these evolution phases, we pointed out that the bump observed during the RGB in the frequency-averaged tidal dissipation for the dynamical tide has no effect on the semi-major axis of close-in Jupiter-mass planets orbiting $1\,M_\odot$ and $1.2\,M_\odot$ stars.

Thanks to these combined developments we now have access to a complete model to follow both the evolution of the tidal dissipation and of the planetary semi-major axis. Indeed, we possess a simplified but robust theoretical prescription for the dynamical tides, and we can follow the internal structure and rotation rate of the star thanks to STAREVOL as well as the planetary orbital evolution using the secular code from Bolmont & Mathis (2016). We can thus use these results to perform modelling of planetary architecture and planetary population synthesis.

The next step will be to directly couple stellar evolution to orbital evolution code using the frequency-averaged tidal dissipation formalism to fully study the possible retro-action of tides and magnetic interactions on the internal structure and rotation of both stars and planets (for instance, using the

prescriptions derived by Strugarek et al. 2014; Strugarek 2016; Bolmont & Mathis 2016; and Gallet et al. 2017). In addition, we will take into account realistic density profiles in the convective envelope of low-mass stars (e.g. from the STAREVOL code). This development will be done by solving the full linearized spectral equations derived by Ogilvie (2013) for densities that vary with radius. Finally, in this work we only included the dissipation of tidal inertial waves inside the convective envelope of rotating low-mass stars. The next step will be to extend this analysis to tidal dissipation inside the radiative core of these stars (Ivanov et al. 2013; Guillot et al. 2014), hence completing the present partial physical description. Other dynamical processes such as the effects of differential rotation on tides should also be taken into account (e.g. Favier et al. 2014; Guenel et al. 2016). In this framework, frequency-averaged and frequency-dependent dissipation should be considered.

References

Albrecht, S., Winn, J. N., Johnson, J. A., et al. 2012, ApJ, 757, 18
Amard, L., Palacios, A., Charbonnel, C., Gallet, F., & Bouvier, J. 2016, A&A, 587, A105
Asplund, M., Grevesse, N., Sauval, A. J., & Scott, P. 2009, ARA&A, 47, 481
Auclair-Desrotour, P., Le Poncin-Lafitte, C., & Mathis, S. 2014, A&A, 561, L7
Barker, A. J., & Ogilvie, G. I. 2009, MNRAS, 395, 2268
Barker, A. J., & Ogilvie, G. I. 2010, MNRAS, 404, 1849
Bolmont, E., & Mathis, S. 2016, Celestial Mech. Dyn. Astron., 126, 275
Bolmont, E., Raymond, S. N., & Leconte, J. 2011, A&A, 535, A94
Bolmont, E., Raymond, S. N., Leconte, J., & Matt, S. P. 2012, A&A, 544, A124
Borucki, W. J., Koch, D., Basri, G., et al. 2010, Science, 327, 977
Bouvier, J., Forestini, M., & Allain, S. 1997, A&A, 326, 1023
Broeg, C., benz, w., fortier, a., et al. 2015, in AAS/Division for Extreme Solar Systems Abstracts, 3, 503.04
Brott, I., de Mink, S. E., Cantiello, M., et al. 2011, A&A, 530, A115
Charbonneau, D., Brown, T. M., Latham, D. W., & Mayor, M. 2000, ApJ, 529, L45
Charbonnel, C., Decressin, T., Lagarde, N., et al. 2017, A&A, 604, A113
Choi, J., Dotter, A., Conroy, C., et al. 2016, ApJ, 823, 102
CoRot Team 2016, The CoRoT Legacy Book: The adventure of the ultra high precision photometry from space, by the CoRot Team (EDP Sciences)
Cranmer, S. R., & Saar, S. H. 2011, ApJ, 741, 54
de Boer, K., & Seggewiss, W. 2008, Stars and Stellar Evolution (Cambridge University Press)
Decressin, T., Mathis, S., Palacios, A., et al. 2009, A&A, 495, 271
Eggleton, P. P., Kiseleva, L. G., & Hut, P. 1998, ApJ, 499, 853
Endal, A. S., & Sofia, S. 1976, ApJ, 210, 184
Endal, A. S., & Sofia, S. 1981, ApJ, 243, 625
Fabrycky, D. C., Lissauer, J. J., Ragozzine, D., et al. 2014, ApJ, 790, 146
Favier, B., Barker, A. J., Baruteau, C., & Ogilvie, G. I. 2014, MNRAS, 439, 845
Ferraz-Mello, S., Tadeu dos Santos, M., Folonier, H., et al. 2015, ApJ, 807, 78
Gallet, F., & Bouvier, J. 2013, A&A, 556, A36
Gallet, F., & Bouvier, J. 2015, A&A, 577, A98
Gallet, F., Charbonnel, C., Amard, L., et al. 2017, A&A, 597, A14
Goldreich, P., & Soter, S. 1966, Icarus, 5, 375
Goldreich, P., & Keeley, D. A. 1977, ApJ, 211, 934
Goldreich, P., & Nicholson, P. D. 1989a, ApJ, 342, 1079
Goldreich, P., & Nicholson, P. D. 1989b, ApJ, 342, 1075
Greenberg, R. 2009, ApJ, 698, L42
Guenel, M., Baruteau, C., Mathis, S., & Rieutord, M. 2016, A&A, 589, A22
Guillot, T., Lin, D. N. C., Morel, P., Havel, M., & Parmentier, V. 2014, EAS Pub. Ser., 65, 327
Hansen, B. M. S. 2010, ApJ, 723, 285
Hansen, B. M. S. 2012, ApJ, 757, 6

---

[4] https://obswww.unige.ch/Recherche/evol/starevol/Galletetal17.php

Howell, S. B., Sobeck, C., Haas, M., et al. 2014, PASP, 126, 398
Husnoo, N., Pont, F., Mazeh, T., et al. 2012, MNRAS, 422, 3151
Hut, P. 1981, A&A, 99, 126
Ivanov, P. B., Papaloizou, J. C. B., & Chernov, S. V. 2013, MNRAS, 432, 2339
Jackson, B., Greenberg, R., & Barnes, R. 2008, ApJ, 678, 1396
Johnstone, C. P., Güdel, M., Brott, I., & Lüftinger, T. 2015, A&A, 577, A28
Kawaler, S. D. 1988, ApJ, 333, 236
Lagarde, N., Decressin, T., Charbonnel, C., et al. 2012, A&A, 543, A108
Lai, D. 2012, MNRAS, 423, 486
Lanza, A. F., & Shkolnik, E. L. 2014, MNRAS, 443, 1451
Lanzafame, A. C., & Spada, F. 2015, A&A, 584, A30
Leconte, J., Chabrier, G., Baraffe, I., & Levrard, B. 2010, A&A, 516, A64
MacDonald, G. J. F. 1964, Rev. Geophys. Space Phys., 2, 467
Maeder, A., & Zahn, J.-P. 1998, A&A, 334, 1000
Mardling, R. A., & Lin, D. N. C. 2002, ApJ, 573, 829
Mathis, S. 2015, A&A, 580, L3
Mathis, S., & Remus, F. 2013, in eds. J.-P. Rozelot, & C. Neiner (Berlin: Springer Verlag), Lect. Notes Phys., 857, 111
Mathis, S., & Zahn, J.-P. 2004, A&A, 425, 229
Mathis, S., Palacios, A., & Zahn, J.-P. 2004, A&A, 425, 243
Mathis, S., Auclair-Desrotour, P., Guenel, M., Gallet, F., & Le Poncin-Lafitte, C. 2016, A&A, 592, A33
Matt, S. P., Brun, A. S., Baraffe, I., Bouvier, J., & Chabrier, G. 2015, ApJ, 799, L23
Mayor, M., & Queloz, D. 1995, Nature, 378, 355
Mazeh, T., Holczer, T., & Faigler, S. 2016, A&A, 589, A75
McQuillan, A., Mazeh, T., & Aigrain, S. 2013, ApJ, 775, L11
Mignard, F. 1979, Moon and Planets, 20, 301
Moutou, C., Boisse, I., Hébrard, G., et al. 2015, in SF2A-2015: Proc. of the Annual meeting of the French Society of Astronomy and Astrophysics, eds. F. Martins, S. Boissier, V. Buat, L. Cambrésy, & P. Petit, 205
Ogilvie, G. I. 2013, MNRAS, 429, 613
Ogilvie, G. I. 2014, ARA&A, 52, 171
Ogilvie, G. I., & Lesur, G. 2012, MNRAS, 422, 1975
Ogilvie, G. I., & Lin, D. N. C. 2004, ApJ, 610, 477
Ogilvie, G. I., & Lin, D. N. C. 2007, ApJ, 661, 1180
Palacios, A., Talon, S., Charbonnel, C., & Forestini, M. 2003, A&A, 399, 603

Palacios, A., Charbonnel, C., Talon, S., & Siess, L. 2006, A&A, 453, 261
Pinsonneault, M. H., Kawaler, S. D., & Demarque, P. 1990, ApJS, 74, 501
Privitera, G., Meynet, G., Eggenberger, P., et al. 2016a, A&A, 591, A45
Privitera, G., Meynet, G., Eggenberger, P., et al. 2016b, A&A, 593, A128
Rauer, H., Catala, C., Aerts, C., et al. 2014, Exp. Astron., 38, 249
Reiners, A., & Mohanty, S. 2012, ApJ, 746, 43
Remus, F., Mathis, S., & Zahn, J.-P. 2012, A&A, 544, A132
Réville, V., Brun, A. S., Matt, S. P., Strugarek, A., & Pinto, R. F. 2015, ApJ, 798, 116
Ricker, G. R., Winn, J. N., Vanderspek, R., et al. 2015, J. Astron. Telesc., Instrum. Syst., 1, 014003
Saar, S. H. 1996, in Stellar Surface Structure, eds. K. G. Strassmeier, & J. L. Linsky, IAU Symp., 176, 237
Saar, S. H. 2001, in 11th Cambridge Workshop on Cool Stars, Stellar Systems and the Sun, eds. R. J. Garcia Lopez, R. Rebolo, & M. R. Zapaterio Osorio, ASP Conf. Ser., 223, 292
Schröder, K.-P., & Connon Smith, R. 2008, MNRAS, 386, 155
Siess, L., & Livio, M. 1999, MNRAS, 308, 1133
Siess, L., Dufour, E., & Forestini, M. 2000, A&A, 358, 593
Siess, L., Izzard, R. G., Davis, P. J., & Deschamps, R. 2013, A&A, 550, A100
Strugarek, A. 2016, ApJ, 833, 140
Strugarek, A., Brun, A. S., Matt, S. P., & Réville, V. 2014, ApJ, 795, 86
Talon, S., & Zahn, J.-P. 1997, A&A, 317, 749
Teitler, S., & Königl, A. 2014, ApJ, 786, 139
Terquem, C., Papaloizou, J. C. B., Nelson, R. P., & Lin, D. N. C. 1998, ApJ, 502, 788
Verbunt, F., & Phinney, E. S. 1995, A&A, 296, 709
Villaver, E., & Livio, M. 2009, ApJ, 705, L81
Winn, J. N., Fabrycky, D., Albrecht, S., & Johnson, J. A. 2010, ApJ, 718, L145
Witte, M. G., & Savonije, G. J. 2002, A&A, 386, 222
Wu, Y. 2005, ApJ, 635, 688
Zahn, J. P. 1966, Annales d'Astrophysique, 29, 489
Zahn, J.-P. 1975, A&A, 41, 329
Zahn, J.-P. 1977, A&A, 57, 383
Zahn, J.-P. 1989, A&A, 220, 112
Zahn, J.-P. 1992, A&A, 265, 115
Zahn, J.-P., & Bouchet, L. 1989, A&A, 223, 112